

Extreme heat and drought typical of an end-of-century climate could occur over Europe soon and repeatedly

Laura Suarez-Gutierrez ^{1,2,3✉}, Wolfgang A. Müller¹ & Jochem Marotzke ¹

Extreme heat and drought typical of an end-of-century climate could soon occur over Europe, and repeatedly. Despite the European climate being potentially prone to multi-year successive extremes due to the influence of the North Atlantic variability, it remains unclear how the likelihood of successive extremes changes under warming, how early they could reach end-of-century levels, and how this is affected by internal climate variability. Using the Max Planck Institute Grand Ensemble, we find that even under moderate warming, end-of-century heat and drought levels virtually impossible 20 years ago reach 1-in-10 likelihoods as early as the 2030s. By 2050–2074, two successive years of single or compound end-of-century extremes, unprecedented to date, exceed 1-in-10 likelihoods; while Europe-wide 5-year megadroughts become plausible. Whole decades of end-of-century heat stress could start by 2040, by 2020 for drought, and with a warm North Atlantic, end-of-century decades starting as early as 2030 become twice as likely.

¹Max Planck Institute for Meteorology, Hamburg, Germany. ²Institut Pierre-Simon Laplace, CNRS, Paris, France. ³Present address: Institute for Atmospheric and Climate Science, ETH Zurich, Zurich, Switzerland. ✉email: laura.suarez@mpimet.mpg.de

Under further global warming, extreme heat will become more frequent, and more extreme¹. Furthermore, currently extremely rare end-of-century events — those that would be average in a much warmer world at the end of the century — can happen earlier than expected due to internal variability. In Europe, this occurred during the 2010 summer, which reached heat levels expected every other year by the end of the century²; but at the time it happened was deemed extremely rare³, remaining the warmest summer observed over most of Europe. Record-shattering extreme heat events that exceed previous records by large amounts will become up to seven times more likely in the next three decades than they were in the recent past⁴. However, we still lack a systematic understanding of how soon typical end-of-century levels of extreme heat and drought stress become a possibility over Europe.

Extreme heat, especially at levels going substantially beyond our previous adaptability range, leads to increased heat-related mortality and morbidity⁵. In the last 30 years, up to 30% of heat-related deaths globally can be attributed to anthropogenic climate change⁶. In addition to the loss of human lives, extreme heat can lead to substantial ecological and socio-economic impacts, such as decreased labor productivity⁷, increased risks of economic losses⁸, wildfires⁹, crop loss¹⁰, and may even render some regions partially uninhabitable¹¹. These far-reaching impacts are exacerbated when maximum temperatures compound with other system stressors¹², such as high humidity¹¹, lack of nighttime cooling¹³, or persistent drought¹⁴. Extreme heat and humidity and insufficient infrastructure caused the death of thousands in the 2015 heatwaves in India and Pakistan¹⁵. In Europe, extreme heat and lack of nighttime cooling brought more than 70,000 additional deaths during the 2003 summer¹⁶. In 2018, the persistent drought and extreme temperatures over Central Europe triggered massive forest mortality events of unprecedented scale¹⁷ and a 50% reduction in agricultural yields¹⁸. The impacts of extreme drought stress are further amplified under an increased volatility between severely dry and wet conditions; which hinders successful water management and accentuates the risk of wildfires, flooding, and mudslides¹⁹.

Furthermore, when these extreme conditions occur repeatedly year after year, they become even more threatening to the already vulnerable socioeconomic and ecological resilience of the region^{12,20–22}. Europe could be especially prone to such year-after-year successive heat and drought extremes, due to the influence of the multi-year variability in the North Atlantic over the European climate^{23–29} acting as a long-term preconditioner. Despite the relevance of their potential cascading impacts and preconditioning in the European climate, it remains unclear how the likelihood of such multi-year successions of extreme heat and drought changes under warming, and moreover, how this likelihood is affected by the internal variability of the climate system.

The intensification of heat and drought, either independently or together, is attributed to be largely anthropogenic and is expected to be accentuated over Europe under further warming^{30–34}. However, changes in the frequency and intensity of heat and drought stress depend not only on the level of global warming; they can also be dampened or amplified by internal variability on interannual to multi-decadal scales^{2,26,33}. For example, the slowly evolving variability in the North Atlantic system affects European temperatures in observations^{35–37}, and modulates past observed trends in concurrent heat and drought over European croplands²⁶. This linkage has been also identified in idealized numerical experiments imposing slowly evolving sea surface temperature (SST) patterns to emulate different phases of Atlantic Multidecadal Variability (AMV), which lead to a marked increase in temperature and slightly lower decrease in precipitation under positive versus negative AMV phases^{27,28}. The

mechanism behind this link involves barotropic wave-train structures driven by the warm North Atlantic states, which in particular for Europe implies dry anticyclonic conditions concurring with near-surface warm-air advection and adiabatic heating^{35,38}.

These oceanic origins of concurrent atmospheric drivers of heat and drought imply a long-term preconditioning on decadal timescales that may make the European climate system particularly prone to such year-after-year successive high-impact heat and drought stress extremes. Moreover, while extreme temperature and precipitation predictions over Europe for the next few months to years remain substantially uncertain; the AMV is thought to be one of the most predictable aspects of decadal climate³⁹. Therefore, improving our understanding of how the relatively predictable AMV affects successive and compounding heat and drought stress is crucial for both the prediction and the attribution of such low-probability, high-impact events. In turn, more robust prediction and attribution of such events would greatly improve our preparedness and the efficiency of our adaptation and mitigation efforts.

We assess how soon different forms of end-of-century heat and drought stress could occur over Europe, and the role that the decadal variability in the North Atlantic plays in this outcome, with a twofold impact-relevant focus. This impact-relevant focus comes, first, from assessing the likelihood of successive, year-after-year extremes; and second, from focusing both on single and compound heat and drought metrics reflecting potential compounding and cascading hazards. Our ultimate goal is to determine how internal climate variability leads to worst-case successive and compounding heat and drought stress accumulating to produce the most extreme decades, and how soon into the near future such heat and drought loaded decades could bring a taste of the end-of-the-century reality.

For this we use cumulative excess metrics that combine the effects of both intensity and persistency of all events within a season⁴⁰, as a sum of every instance beyond a given threshold (see Methods). We expand the existing cumulative heat framework⁴⁰ based on maximum temperatures, here referred to as Excess Heat, to cover three additional excess metrics that reflect extreme summer heat stress and May–October drought stress: Humid Heat, Night Heat, and Rain Deficit. In addition to these four types of single heat and drought stress extremes, we also assess three compound heat and drought stress types: Compound Heat Stress, Compound Heat and Drought, and Drought-Rain Volatility. For this we use the 100-member Max Planck Institute Grand Ensemble (MPI-GE)⁴¹, under historical and RCP4.5 forcing leading to roughly 2.25 C of warming by the end of the century².

MPI-GE is one of the largest existing initial-condition ensembles of a comprehensive, fully coupled Earth System Model currently available. This large ensemble size is crucial for robustly sampling and assessing changes in low-probability univariate events, and it is even more important for multivariate compound events and temporally successive extremes⁴². In addition to its large ensemble size, compared to other large ensembles MPI-GE also offers one of the most adequate representations of the historical internal variability and forced changes in observed temperatures⁴³ and precipitation⁴⁴. For these reasons, MPI-GE is the best-available tool for this first assessment of how soon internal climate variability could bring end-of-century levels of successive extreme heat and drought stress upon Europe.

Results and discussion

Excess heat and drought projections. By the end of the 21st century and even under moderate warming, extreme heat and

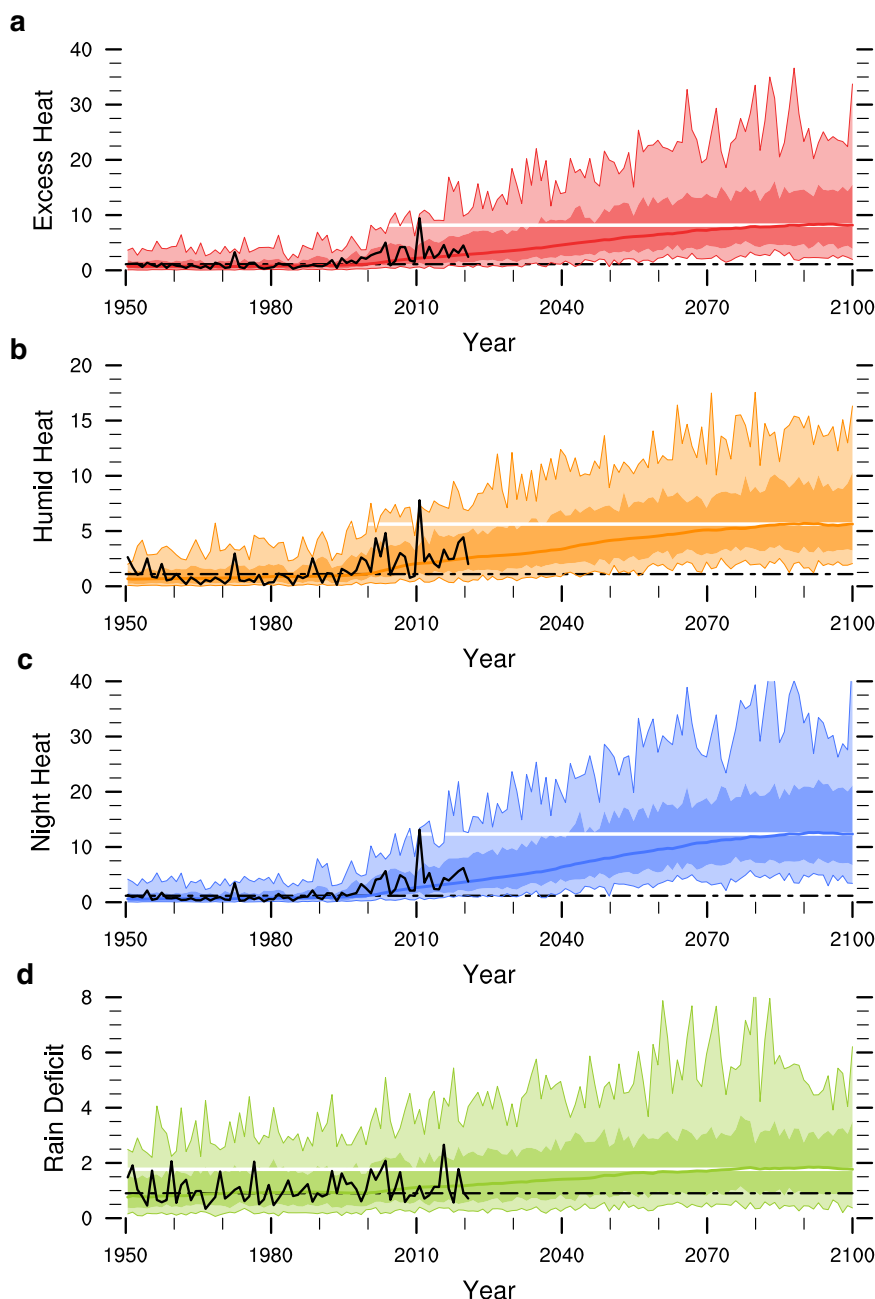


Fig. 1 Excess Heat and Drought Metrics for MPI-GE against E-OBS Observations. Time series of June–August Summer (a) Excess Heat, (b) Humid Heat, (c) Night Heat, and (d) May–October Rain Deficit (see methods for metric definitions) simulated by MPI-GE (color) against E-OBS observations (black; 1950–2021). Light shading represents the full ensemble spread; dark shading represents the 10th–90th percentile range of the ensemble. Thick colored lines show the 10-year average of the 50th percentile of the ensemble. The black dashed line represents this 50th percentile at the end of the 20th century, averaged over the period of 1990–1999; while the white line represents this 50th percentile the end of the 21st century, averaged over 2090–2099. Each metric is shown as a ratio with respect to its average over the period of 1950–1999, and is averaged over the European region defined by the [35–63 N, 10W–55E] domain. MPI-GE simulations are historical (1950–2005) and RCP4.5 (2006–2099) and subsampled to land grid cells where observations are available.

drought stress is projected to increase intensely over Europe, with practically all simulated years exhibiting levels well beyond recent-past average conditions as early as 2040 (Fig. 1). However, and even more importantly, worst-case years at the upper tails of the distributions show an even more marked increase than the average, with deviations from their concurrent average climate of unprecedented scale. For all heat metrics, typical end-of-century extremes, defined as the MPI-GE 2090–2099 average, become plausible albeit rare already in 2000–2009 in MPI-GE, and were exceeded in E-OBS observations in 2010. MPI-GE simulates

summers as extreme as the 2010 record already 5–10 years prior, showing that MPI-GE is able of capturing the timing and intensity of the most extreme events on the observational record. These end-of-century summers, virtually impossible only 20 years ago and a rare occurrence in the last decades, reach 1-in-10 chances already in 2030–2039 for all heat metrics.

For a typical end-of-century summer, Excess Heat reaches values almost 10 times as high as the 1950–1999 average, while extreme end-of-century summers at the upper tail of the distribution (beyond 90th percentile) reach values 20 to 35 times

as high, with similar tendencies for Night Heat. For Humid Heat, this increase is less marked and the upper tail summers reach levels 10–15 times higher than the 1950–1999 average, with somewhat smaller differences between average and higher-percentile summers. For excess Rain Deficit, the distribution is centered around values roughly twice as large as the recent past average by the end of the century. The most extremely dry years reach rain deficits 3 to 8 times higher than the 1950–1999 average. Thus, all forms of extreme heat become more prevalent and intense by the end of the century than in the recent past; while rain deficits below current-climate thresholds suffer a less substantial increase in comparison in MPI-GE.

These projections are based on an adequate representation of the magnitude, variability and forced changes under warming in E-OBS observations by MPI-GE for all excess metrics in the period of 1950–2021 (Supplementary Fig. 1). Our evaluation shows that E-OBS observations are mostly within the ensemble spread and well within the perfect model range of MPI-GE (further details on this evaluation framework described in ref. 43). In the observed period, 2010 stands out as the summer exhibiting the most extreme heat over Europe. It reached heat levels 10 times higher than the 1950–1999 average across all metrics, and roughly coincides with the 1-in-100-members ensemble maxima for the concurrent period. For Rain Deficit, 2015 stands out as the year with the most extreme lack of precipitation, roughly coinciding with the 90th percentile of the ensemble distribution. However, none of the observed rain deficits are quite as extreme as concurrent MPI-GE ensemble maxima, indicating that MPI-GE may overestimate the risk and magnitude of rain-deficit drought, or that an event as rare on a continental-scale has not yet occurred.

Typical end-of-century extreme heat has a less than 5% chance of occurring during any single year in the 2000–2024 period (Fig. 2). In the next 25 years this likelihood increases to 10–15%, meaning that one or more summers in every 10 could exceed end-of-century levels, with the highest likelihoods over Central

and Northern Europe for all heat metrics (Supplementary Fig. 2). By 2050–2074, this likelihood rises to more than a third. Moreover, the likelihood that after one of such end-of-century extreme summers we experience another one goes from virtually zero to 2–4% in the next 25 years. By 2050–2074, the likelihood of two successive summers of end-of-century heat exceeds 15%, with up to a 3% chance of year-after-year end-of-century extreme heat occurring for 5 consecutive years. On the other hand, the likelihood of end-of-century rain deficit drought stress stands at 20% during recent decades, and rises to over 30% in the next 25 years. The likelihood of two consecutive years of end-of-century drought stress caused by an extreme lack of rain almost triples in the next 25 years compared to the recent past to almost 15%. Lastly, with likelihoods over 3.5% by 2050–2074, unprecedented 5-year long mega-droughts affecting the whole European continent, although rare, become plausible.

The likelihood of end-of-century extremes compounding in any given year also becomes substantially higher in the next decades (Fig. 3). A single year of end-of-century Compound Heat Stress or Compound Heat and Drought, both extremely rare combinations in the recent past, could occur during one out of every 10 summers in the next 25 years, and roughly 1 out of every 3 by 2050. The likelihood of experiencing successive end-of-century compound extremes for two consecutive years, virtually zero in the recent past, rises to over 1-in-10 in the 2050–2074 period. And while compound year-after-year extremes for 5 consecutive summers remain rare, they could by then become plausible, with roughly a 1–2% likelihood. Drought-Rain Volatility, reflecting years of extreme Rain Deficit followed or preceded by years of extreme Rain Excess (see Methods) becomes also twice as likely in the next 25 years, and by 2050–2074 could happen a third of the time.

Distance to end-of-century decades and the influence of the North Atlantic Variability. Accumulated over 10-year periods, decadal excess heat and drought stress varies widely for the

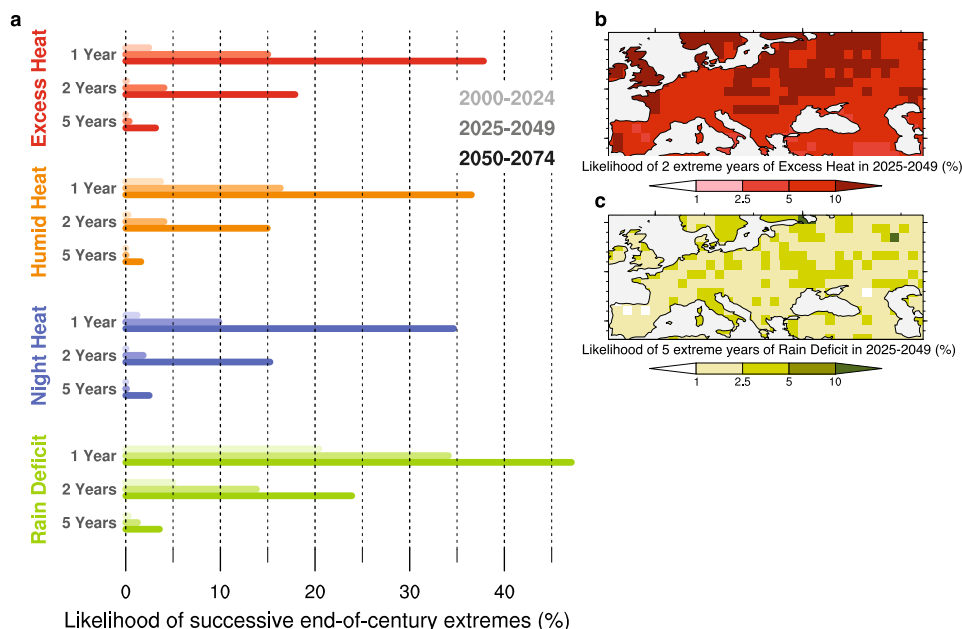


Fig. 2 Likelihood of successive end-of-century extremes. **a** Likelihood of extremes occurring in one year, and that the following 2 or 5 years, also exhibit extreme excess metrics, for the periods of starting in the years 2000–2024 (light colors), 2025–2049 (medium colors) and 2050–2074 (dark colors). Spatial distribution of the likelihood of **(b)** 2 years of extreme Excess Heat and **(c)** 5 years of extreme Rain Deficit in 2025–2049 (for all metrics and extreme year frequencies see Supplementary Fig. 2). Extreme years are defined as those with levels equal or larger than the end-of-century 50th ensemble percentile averaged over the period of 2090–2099.

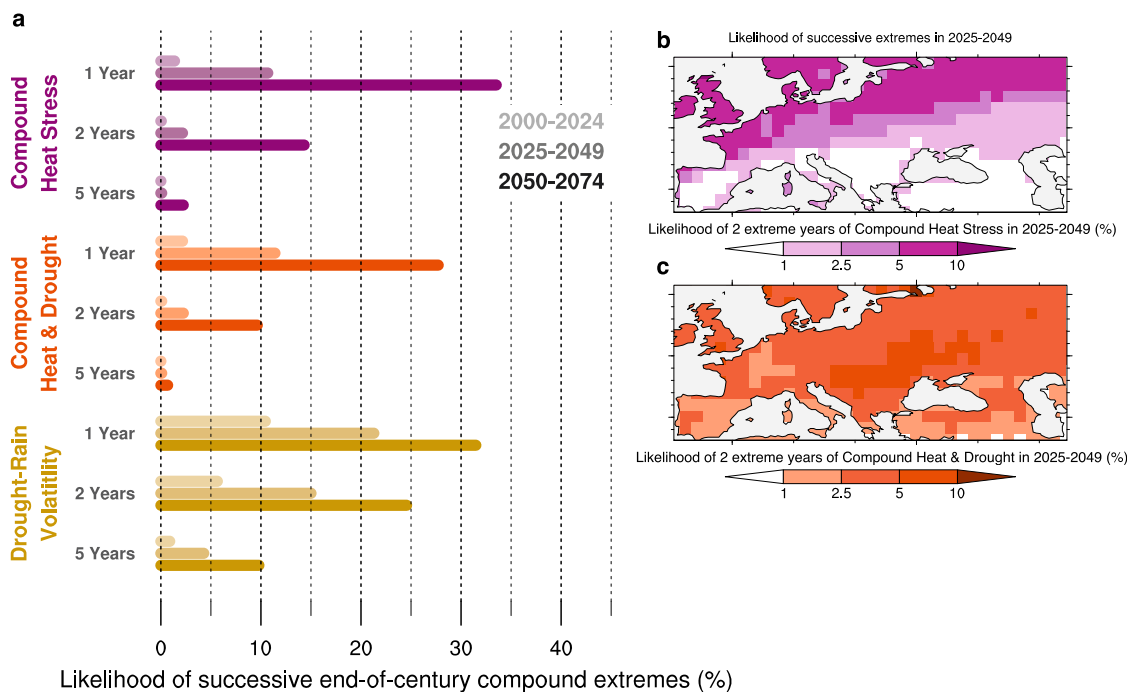


Fig. 3 Likelihood of successive end-of-century compound extremes. **a** Likelihood of compound extremes occurring in one year, and that the following 2 or 5 years also exhibit compound extremes, for the periods starting in the years 2000–2024 (light colors), 2025–2049 (medium colors) and 2050–2074 (dark colors). Spatial distribution of likelihood of **(b)** 2 years of extreme compound Heat Stress and **(c)** compound Heat & Drought in 2025–2049 (for all metrics and extreme year frequencies see Supplementary. Fig. 3). Years of Compound Heat Stress are those exhibiting extreme Excess Heat and extreme Night Heat and/or Humid Heat. Years of extreme Compound Heat and Drought are those exhibiting both extreme Excess Heat and Rain Deficit. Years of Drought-Rain Volatility are those exhibiting extreme Rain Deficit plus extreme Excess Rain the year before and/or the year after. Extreme years are defined as those with values equal or larger than the end-of-century 50th ensemble percentile averaged over the period of 2090–2099.

same global warming levels, simply due to internal variability. Furthermore, the range of excess heat and drought stress that is possible in any given decade increases drastically under warming (Fig. 4). The decadal variability in these heat and drought excess metrics becomes so large that it can bring typical end-of-century conditions upon Europe already in the next few decades. Starting in 2040, 5–10% of the decades simulated by MPI-GE exceed end-of-century levels for all heat metrics, and this occurs already in 2020–2029 for Rain Deficits. By 2060, the chances of heat and drought loaded decades that exceed typical-end-of-century levels rise to more than a 1 out of 10.

This wide range of decadal excess heat and drought stress indicates that, depending on the state of internal variability, some decades have a stronger tendency toward successive extreme heat and drought stress than others. And these decadal differences are heavily dominated by the state of the internal variability of the North Atlantic climate system, as defined by its 10-year average SST-based AMV index (Methods). Positive AMV phases lead to an over 100% increase in the likelihood of exceeding typical end-of-century decadal heat stress already in the next decades (Fig. 5). The largest and most wide-spread increase in likelihood occurs for Humid Heat, followed by Night Heat, indicating that warm North Atlantic states increase the likelihood of concurrent heat and high humidity and night-time heat persistence, two of the forms of heat stress mostly linked to human heat-related morbidity. In contrast, the effect of AMV on Rain Deficit does not explain as much of this decadal variability as it does for extreme temperatures and shows larger regional differences in MPI-GE. Typical end-of-century rain deficits are 25% more likely under positive AMV phases over Southern Europe and parts of Eastern Europe, but 10–25% more likely over parts of South-Eastern Europe under negative AMV.

A warm North Atlantic not only makes extreme decades for any given heat excess metric more likely, it also increases the likelihood of decades of compound end-of-century levels for two different forms of heat and drought stress occurring together (Fig. 6). During positive AMV phases, there is over a 1-in-10 chance of decades exceeding typical end-of-century levels already in 2030–2049 for compound day and nighttime Heat Excess, Humid and Night Heat and Heat and Drought. Heat and drought loaded decades exceeding end-of-century levels are twice as likely under positive versus negative AMV phases, and the most extreme decadal heat stress levels in all its forms occur always under warm North Atlantic states.

Conclusions

We quantify how soon different forms of end-of-century heat and drought stress could occur over Europe, and the role that internal climate variability plays in producing the worst-case single, successive, and compounding end-of-century heat and drought. Our results are based on MPI-GE simulations, which are well in agreement with the variability and forced changes in observed excess temperature⁴³ and precipitation⁴⁴ and with the IPCC projections of changes in heat and drought extremes¹. MPI-GE, one of the largest ensembles currently available, provides a precise sampling of low-probability events which is crucial for our analysis. This precise sampling of internal variability is especially key to robustly capture concurrent extreme conditions in more than one variable, or the conditional probabilities of experiencing extreme conditions again after an already extreme year. Furthermore, fully coupled Earth system model simulations that sufficiently capture the effect and variability of large-scale and long-term drivers, such as those of oceanic origin, are key to

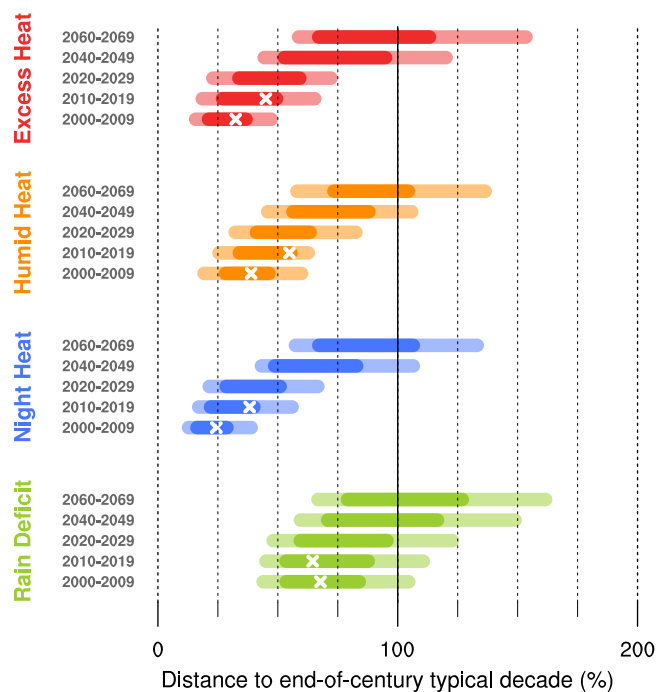


Fig. 4 Distance to end-of-century decades of heat and drought stress.

Variability in excess metrics accumulated over a decade for the whole MPI-GE ensemble spread (pale colors) and for the range between the 10th to 90th percentiles of the ensemble distribution (bright colors), shown as distance to a typical end-of-century decade. White crosses mark the same values but for observed decadal excess in E-OBS. Decadal excess metrics are calculated as the 10-year sum of the annual excess metrics. The distance to the end of the century average decade is calculated as the ratio between each decadal excess metric divided by the 50th ensemble percentile decadal excess in 2090–2099, transformed to percentage. Thus, values of 100% indicate reaching end-of-century typical decades, while values higher than 100% indicate exceeding the levels of end-of-century typical decades. This distance is calculated against the ensemble 50th percentile both for each ensemble member and E-OBS.

robustly assess the changing likelihood of such successive and compounding extremes.

To put these single-model results in context, with a moderate climate sensitivity of $2.8\text{ }^{\circ}\text{C}^{45}$, MPI-GE is largely in agreement with multi-model projections for summer heat extremes, for which we have high confidence on both the sign and intensity of the projected changes¹. In particular, across different climate models, MPI-ESM exhibits one of the lowest biases in reproducing observed temperature extremes⁴⁶, and projects changes in the characteristics of such extremes in line with other models⁴⁷. The results presented here also show good agreement with previous studies assessing observed extreme heat with comparable cumulative heatwave metrics, both in terms of the regions where the largest changes have occurred or are projected to occur and the intensity of the most extreme observed events^{40, 48,49}. Furthermore, the normalized approach of assessing the likelihood of reaching typical end-of-century extreme heat levels makes our single-model results based on MPI-GE extendable to other climate models and valid in a general way (Supplementary Fig. 5). For precipitation changes, MPI-GE shows a drying trend in the May–October season over the region of study comparable to other climate models (Supplementary Fig. 5). However, there is larger inter-model differences in the direction and magnitude of rain-deficit drought changes and lower signal-to-noise ratios in those changes over Europe, which highlights the relevance of

contrasting the results presented here for extreme drought changes with other climate models.

Our findings show that even under moderate warming, unprecedented levels of heat and drought stress typical of an end-of-century climate swiftly become a possibility over Europe in the near-term future. All heat stress forms considered are projected to reach or surpass end-of-century levels that were virtually impossible 20 years ago with a 1-in-10 likelihood as early as during the 2030–2039 decade. Moreover, succeeding extremes of end-of-century extreme single and compound heat and drought stress occurring repeatedly year after year, something that has not yet happened once in the observational record, becomes possible already in the next 30 years, with more than a 1-in-10 likelihood by 2050–2074. By then, two successive years of end-of-century rain-deficits are projected to occur 20% of the time, and there is a non-negligible chance of 5-year long continental scale mega-droughts.

Internal climate variability could bring any of these devastating occurrences typical of an end-of-the-century climate to Europe sooner than expected. This internal variability characterizes all the plausible summers that we could come to experience under the same global warming levels, and this range of plausible summers is growing wider by the decade. The range of potential heat and drought stress accumulated over a whole decade increases to the point that experiencing heat and drought loaded decades typical of an end-of-century climate could become a reality in Europe as early as 2040. This growing range of decadal variability in heat and drought stress over Europe is heavily influenced by the North Atlantic decadal variability. Our results show that under a concurrent warm North Atlantic state, exceeding end-of-century single and compound heat and drought stress during decades starting as early as in 2030 is twice as likely than under a cold North Atlantic state. This link between the comparatively highly predictable North Atlantic heat variability and such nearly impossible to predict multi-year periods of extreme heat and drought stress occurring well ahead of their time provides vital insights to increase our preparedness to some of the upcoming threats of climate change.

Methods

Observational and model data. The model simulations used here are fully-coupled, transient climate simulations from the MPI-GE⁴¹ under historical and RCP4.5 forcing for the periods of 1950–2005 and 2006–2099, respectively. MPI-GE consists of 100 realizations of the same Earth System Model (MPI-ESM1.1), which is fairly similar to the CMIP6 version MPI-ESM1.2 and has a climate sensitivity of $2.8\text{ }^{\circ}\text{C}^{45}$. All of the 100 realizations use the same model physics and parametrizations and are driven by the same external forcings, but each start from a different initial climate state in 1850 taken from different points of the model's pre-industrial control run. MPI-ESM1.1 is used in the low-resolution configuration, with resolution T63 and 47 vertical levels in the atmosphere and 1.5° resolution and 40 vertical levels in the ocean.

Observational data from the E-OBS⁵⁰ dataset version EObsv24.0e for the period of 1950–2021 are used for comparison and evaluation of the MPI-GE simulations against current climate conditions. E-OBS data, with a native regular grid of 0.25° , are regridded to the coarser resolution of MPI-GE simulations. All spatial averages are calculated over land-only grid cells in the European area defined by the $[35\text{--}63\text{ N}, 10\text{W}\text{--}55\text{E}]$ latitude-longitude domain. When comparing against observations, model data are subsampled to grid boxes where observations are available. Note that this version of the E-OBS dataset includes input of several station series that have not been homogenized, and should be used with caution for the evaluation of trends⁵⁰.

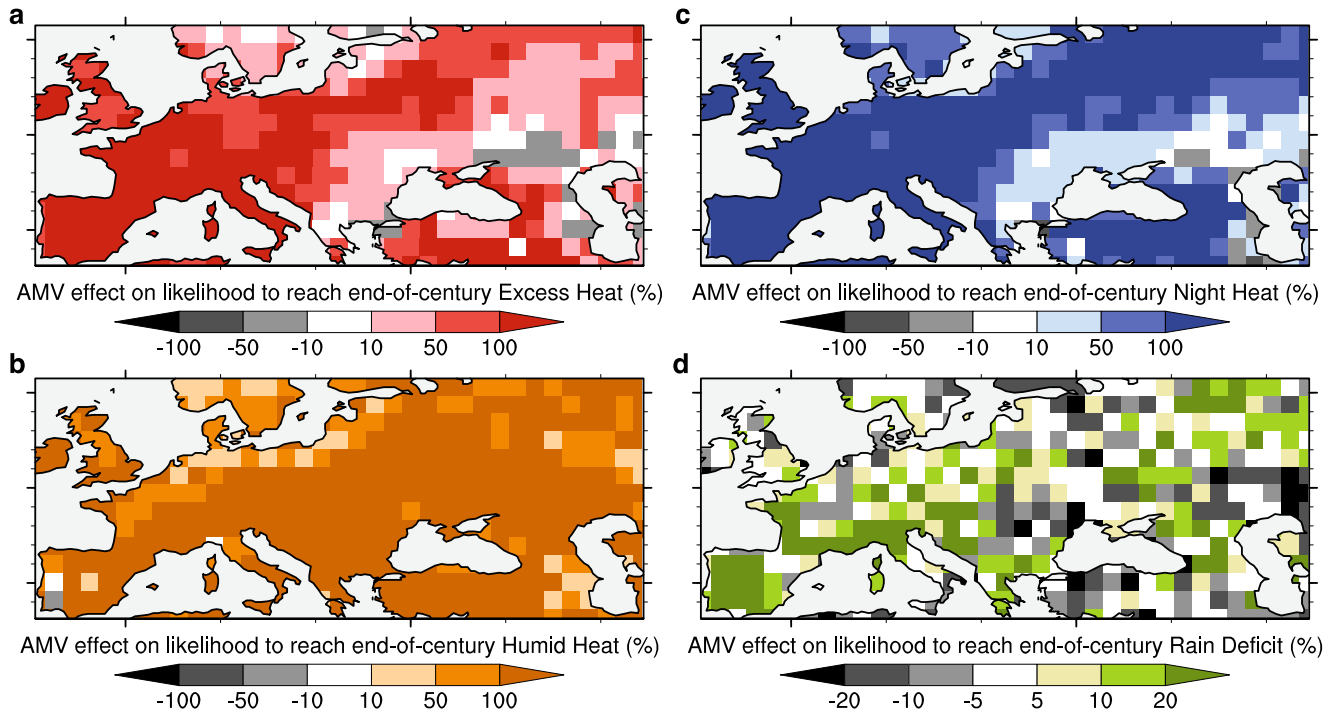


Fig. 5 Effect of AMV phase on likelihood of reaching end-of-century heat and drought levels. **a–d** Weighted difference in likelihood of different decadal excess metrics starting in 2030–2049 reaching typical end-of-century levels under different concurrent AMV phases. This difference is shown as likelihood during AMV+ minus during AMV-, weighted by likelihood during AMV-, in percentage. AMV is defined as the concurrent 10-year running mean of North Atlantic SSTs. Distances to typical end-of-century decades are shown as the decadal excess metric at each grid cell minus the ensemble mean decadal excess in 2090–2099, also at each grid cell (see Supplementary Fig. 4 for non-weighted AMV-phase likelihoods and differences).

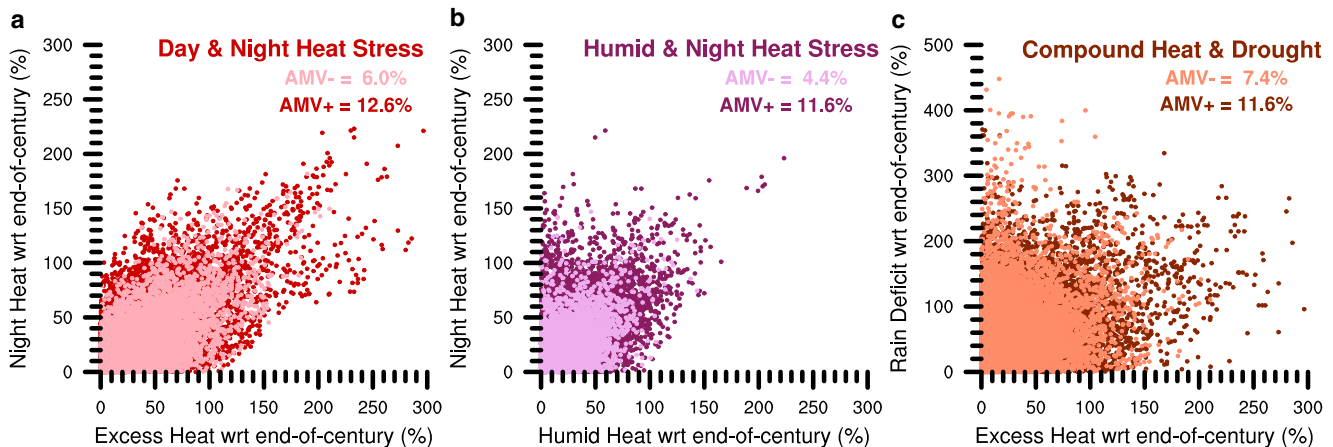


Fig. 6 Effect of AMV phase on likelihood of end-of-century compound extremes. **a–c** Decades exceeding typical end-of-century levels in several heat and drought stress excess metrics under AMV+ (dark dots) and AMV- (light dots), starting in 2030–2049. Each dot represents one decade over one grid cell. Percentages show decades that exceed end-of-century levels under each AMV phase, at grid-cell level. AMV is defined as the concurrent 10-year running mean of North Atlantic SSTs. Distances to typical end-of-century decades are calculated as the difference between each year excess values minus the decadal ensemble average over the period of 2090–2099, divided by the end-of-century average and transformed to percentage.

Heat and drought stress definitions. We use three heat stress indicators based respectively on summer (JJA) daily maximum temperatures, wet bulb temperatures reflecting the combined effect of heat and humidity, and daily minimum temperatures reflecting nighttime heat persistence; and one meteorological drought metric based on May-to-October accumulated monthly precipitation. This meteorological drought metric is calculated based on exceedance of grid-cell based drought thresholds (see section below for further details) to capture to the regional differences in the domain. This spatially consistent definition as well as the focus on the wider May–October season and the

comparison with end-of-century drought levels ensures an adequate representation of the meteorological drought conditions both in the Northern as in Southern parts of the European domain^{51,52}. Wet bulb temperature is a multivariable metric calculated using daily average near-surface 2 m air temperatures and relative humidity based on the method described in ref. ⁵³. Ideally, to obtain the most accurate wet bulb temperatures it should be calculated instantaneously at the model time step. However, this is not possible in MPI-GE, with currently only daily mean relative humidity output available. This approach can lead to a slight overestimation of absolute daily mean wet bulb

temperatures based on instantaneous values⁵⁴, thus we base our analysis solely on relative changes and not on absolute values.

Excess metrics for heat and drought. Although a plethora of possible extreme heat and drought stress metric exists^{1,40,48,49,55}, we choose cumulative metrics based on excess above thresholds specific to the region and time of the year to better capture the effect of both intensity and persistency of these extreme conditions⁵⁵, as well as the extreme conditions that are more relevant for exposure to these hazards and associated adverse impacts⁴⁰. While different measures of average intensity are the base for most common heat metrics, metrics based on cumulative values of the exceedances above a given threshold offer a more unequivocal approach and a better comparison of events of different length and spatial extent. Furthermore, the impact of heat and drought stress is primarily determined by the accumulation of heat and drought levels that exceed a certain level experienced over a specific time period, rather than by averaged values⁵⁵. Moreover, this level above which exceedance yields most adverse impacts should be based on a threshold that defines extreme conditions for each specific region and time of the year, as done here, rather than anomalies with respect to mean climatological values, to better reflect the potential ecological and socioeconomic impacts of such events^{40,55}.

Thus, applying these best-practice principles and based on the heat and drought stress indicators described above, we use excess metrics that capture excess extreme heat and drought exceeding certain region and time specific extreme thresholds, accumulated over whole seasons. For heat-related excess metrics (i.e., Excess Heat, Humid Heat, and Night Heat) we calculate for each grid cell and day, the difference between the actual temperature reached (maximum daily temperature, wet bulb temperature, or minimum daily temperature for each metric, respectively) minus the given temperature threshold over said grid cell (Eq. (1)). Each heat excess metric is then calculated as the sum of these differences for all days above threshold per summer (JJA, Eq. (1)), expanding on the accumulated heat metric for maximum temperatures *cumulative heat* described in ref. ⁴⁰. This can be expressed as:

$$\text{Excess Heat Metric} = \sum_{i=1}^j \sum_{d=1}^n (\text{Temperature} - \text{Threshold}) \quad (1)$$

where Excess Heat Metric represents each heat based excess metric (i.e., Excess Heat, Humid Heat, and Night Heat), j is the number of grid cells, n is the number of heat above threshold days in a JJA season, Temperature corresponds to the three temperature-based variables used (maximum daily temperature, wet bulb temperature, or minimum daily temperature for each metric, respectively) at the grid cell level and Threshold is the pooled daily 90th percentile level in this Temperature, also at the grid cell level. We calculate this Threshold under historical conditions defined by the period of 1950–1999, to allow a comparison with E-OBS observations. Note that this difference between the Temperature and Threshold is only summed if it is positive, namely only for days and grid cells exhibiting extreme heat conditions of heat threshold exceedance.

Excess rain deficit is calculated similarly (Eq. (2)), but based on the difference between the monthly 10th percentile drought-threshold minus the actual monthly cumulative precipitation at each grid cell, for each month in the May-to-October period each year³², expressed as:

$$\text{Rain Deficit Metric} = \sum_{i=1}^j \sum_{m=1}^n (\text{Threshold} - \text{Precipitation}) \quad (2)$$

Where j is the number of grid cells, n is the number of drought months days in a May–October season, Threshold is the monthly 10th percentile of monthly accumulated precipitation for each

month in the May–October period at the grid cell level, and Precipitation is the actual accumulated precipitation value for each given month and grid cell. Again, we calculate this Threshold under historical conditions defined by the period of 1950–1999, to allow a comparison with E-OBS observations, and again only positive differences, namely only months with Precipitation values below this Threshold, are summed.

Using more extreme thresholds (e.g., 95th percentile for temperature-based extremes and 5th percentile for precipitation-based extremes) to calculate these excess metrics does not lead to substantially different results, since both the end-of-century levels and the past of near-term future exceedances are based on the same percentile-based relative definitions (Supplementary Fig. 6).

For climatological reference period we use the period of 1950–1999, a longer period that spans further into the past than the commonly used 30-year reference periods. This longer period is crucial to allow a robust quantification of the thresholds used to define extreme conditions. It ensures that the thresholds calculated here are not (1) overly confounded by the effect of the rising trend in heat and drought in the last years of the reference period, (2) skewed by any potential extreme events occurring within the reference period, and (3) biased by the potential effect of subdecadal to multidecadal variability in the climate system.

Compound excess metrics (i.e., Compound Heat Stress, Compound Heat and Drought, and Drought-Rain Volatility), are based on the same excess metrics co-occurring over their respective seasons (JJA for heat metrics and May–October season for precipitation metrics), or in the following or preceding year for Drought-Rain Volatility. Compound Heat Stress reflects Excess Heat and concurrent Humid Heat and/or Night Heat extreme conditions occurring together on any given summer. Compound Heat and Drought reflects simultaneous extreme summer Excess Heat and May–October Rain Deficit conditions. Drought-Rain volatility reflects years of extreme Rain Deficits followed or preceded by years of extreme Rain Excess. Rain Excess is defined similar to the heat excess metrics (Eq. (1)) but as the difference in monthly cumulative precipitation minus the 90th percentile in monthly precipitation for each month and grid cell in the whole year.

Definition of extreme years and distance to end-of-century levels. We define extreme years in each excess metric as those years exceeding the typical end-of-century levels defined by the 50th percentile of the ensemble spread, averaged over the period of 2090–2099. For the analysis in Figs. 2 and 3 we consider events with probabilities below 1% to be virtually impossible and to have virtually zero or negligible likelihoods, while likelihoods above 1% are considered non-negligible and thus events with likelihoods above 1% are here considered plausible.

Typical end-of-century levels for decadal metrics, characterized by their start year, are defined as the 50th percentile of the ensemble distribution in 2090. Therefore, the distance to an end-of-century typical decade (Eq. (3)) used in the analysis in Figs. 4, 5, and 6 is calculated as the distance between the decadal metric on any given start year and this 50th percentile in the decadal metric ensemble distribution in 2090, described as:

$$\text{EOCDistance}_{i,m} = \text{Dec_Metric}_{i,m} - \text{Dec_Metric}_{2090-2099,50thp} \quad (3)$$

Where $\text{EOC_Distance}_{i,m}$ is the distance to the end-of-century typical value for a given decade i and member m , as the difference between the $\text{Dec_Metric}_{i,m}$, the yearly excess metric summer over

all years for the given decade for the given member, and the typical end-of-century level defined as the sum over the end-of-century decade 2090–2099 of the 50th percentile of the Metric across all ensemble members. This calculation is based on spatially aggregated metrics, except for map-based figures which use metrics and end-of-century values at the grid cell level. For visualization purposes, in Fig. 4 we show this distance as a ratio, thus dividing the decadal metric on any given start year by the end-of-century 50th percentile in the decadal metric ensemble distribution in 2090, and transform it to percentage. For assessments at the grid-cell level in Figs. 5 and 6, we substitute the 50th percentile of the ensemble for the ensemble mean for computational efficiency, since both metrics yield comparable results.

Multi-model comparison of extreme temperature and rain deficit changes. We assess the dependence of our results on the choice of climate model used, to frame the changes seen in MPI-GE in heat and precipitation-deficit drought extremes over Europe in a broader multi-model context. For this, we analyze the evolution and comparable end-of-century levels for a simplified version of the metrics used in this study across several other large ensembles, namely ACCESS-ESM1.5, CanESM5, and MIROC6 (Supplementary Fig. 5). We use these three additional ensembles for three main reasons: first, they have an ensemble size of a minimum of 40 members. Second, they all provide simulations under forcing conditions (SSP245) comparable to the original RCP4.5 used in our study. And third, they cover a wide range of different equilibrium climate sensitivities to sample different warming responses (ACCESS-ESM1.5: 3.9K, CanESM5: 5.7K, MIROC6: 2.6K, MPI-GE: 2.8K).

To assess comparable end-of-century levels across these climate models with different warming rates, we use a common warming level of 2C of global mean surface temperature increase (GMST) above pre-industrial conditions. The comparable typical end-of-century extreme heat and drought levels refer in this case to a 2C warmer world (instead of the 2.25C of GMST increase in our main analysis corresponding to actual end-of-century levels in MPI-GE), and is calculated as an average of the 10-year periods after each model exceeds the 2C GMST increase levels. This multi-model comparison (Supplementary Fig. 5) shows that, over Europe, MPI-GE shows a slightly lower increase in TXx anomalies compared to the models considered, and a drying signal that is of similar magnitude as in MIROC6 and slightly less strong than in ACCESS-ESM1.5. In contrast, CanESM5 projects a precipitation increase over this region, with even the driest May–October seasons exhibiting similar or more accumulated precipitation levels than the 1950–1999 average. This decrease in drought conditions in CanESM5 is not in line with the latest IPCC consensus, which indicates an increase in drought conditions for this region¹.

The comparable end-of-century extreme temperature levels cluster around 5C for the higher warming rate models ACCESS-ESM1.5 and CanESM5 and around 4C for the lower warming rate models MIROC6 and MPI-GE. However, all four models project the first plausible exceedance of their relative comparable end-of-century levels within less of ten years difference from when this first exceedance occurs in MPI-GE. For precipitation changes our results show large inter-model differences, both for the comparable end-of-century drought levels and for when the different models project the first plausible exceedance of such levels. For precipitation deficit extremes we visualize this first plausible exceedance for five successive years, since all models including MPI-GE show occurrences of the end-of-century drought levels from the beginning of the historical simulations due to the lower

signal-to-noise ratios in precipitation changes compared to temperature changes.

In summary, this multi-model assessment indicates that for heat extremes the normalized approach of reaching end-of-century extremes makes our single-model results valid for other climate models. For drought extremes, the larger inter-model differences in the direction and magnitude of changes and the lower signal-to-noise ratios in those changes make our results more model dependent, although the change in drought conditions in MPI-GE is well in line with other climate model projections.

Atlantic multidecadal variability index definition. To capture the internal multi-year variability in North Atlantic temperatures, we use an AMV index defined as the 10-year mean SST in the region defined by the [20–60N, 70W–20W] latitude-longitude box. To remove forced effects we detrend each SST simulated time series by removing the ensemble mean at each grid cell⁵⁶, and normalize it by dividing it by its standard deviation. AMV phases are selected for start years when this AMV index is equal or larger to half standard deviation for positive phases, and equal or smaller than minus half standard deviation for negative phases.

Data availability

The data required to interpret the findings reported in this article is available in the public long-term archive repository of the German Climate Computing Center (DKRZ-LTA; https://www.wdc-climate.de/ui/entry?acronym=DKRZ_LTA_1152_ds00903) and in the public repository Zenodo (<https://doi.org/10.5281/zenodo.10044343>). The source MPI-GE simulations and model output are partially available for download at <https://esgf-data.dkrz.de/projects/mp-ge/> or by contacting grandensemble@mpimet.mpg.de. E-OBS observational data are available for download at <https://www.ecad.eu/download/ensembles/download.php>.

Code availability

The scripts used to perform this analysis and other supporting information that may be useful in interpreting and reproducing this work are available in the public long-term archive repository of the German Climate Computing Center (DKRZ-LTA; https://www.wdc-climate.de/ui/entry?acronym=DKRZ_LTA_1152_ds00903) and in the public repository Zenodo (<https://doi.org/10.5281/zenodo.10044343>). The analysis and figures in this article were performed using Climate Data Operator (CDO) software⁵⁷, Python and NCAR Command Language (NCL, NCAR 2019; Version 6.6.2).

Received: 28 March 2023; Accepted: 27 October 2023;

Published online: 30 November 2023

References

1. Seneviratne, S. I., et al. Weather and Climate Extreme Events in a Changing Climate. In *Climate Change 2021: the physical science basis. contribution of working Group I to the Sixth Assessment Report of the Intergovernmental Panel on Climate Change* (eds. Masson-Delmotte, V., P. Zhai, A. Pirani, S. L. Connors, C. Péan, S. Berger, N. Caud, Y. Chen, L. Goldfarb, M. I. Gomis, M. Huang, K. Leitzell, E. Lonnoy, J. B. R. Matthews, T. K. Maycock, T. Waterfield, O. Yelekçi, R. Yu, and B. Zhou) (Cambridge University Press, Cambridge, United Kingdom and New York, NY, USA, 1513–1766, 2021).
2. Suarez-Gutierrez, L., Li, C., Müller, W. A. & Marotzke, J. Internal variability in European summer temperatures at 1.5C and 2C of global warming. *Environ. Res. Lett.* **13**, 064026 (2018).
3. Barriopedro, B., Fischer, E. M., Luterbacher, J., Trigo, R. M. & G.-Herrera, R. The hot summer of 2010: redrawing the temperature record map of Europe. *Science* **332**, 220–224 (2011).
4. Fischer, E. M., Sippel, S. & Knutti, R. Increasing probability of record-shattering climate extremes. *Nat. Clim. Change* **11**, 689–695 (2021).
5. Watts, N. et al. The 2020 report of the lancet countdown on health and climate change: responding to converging crises. *Lancet.* **397**, 129–170 (2021). 9.
6. Vicedo-Cabrera, A. M. et al. The burden of heat-related mortality attributable to recent human-induced climate change. *Nat. Clim. Change* **11**, 492–500 (2021).

7. Orlov, A., Sillmann, J., Aunan, K., Kjellstrom, T. & Aaheim, A. Economic costs of heat-induced reductions in worker productivity due to global warming. *Global Environ. Change* **63**, 102087 (2020).
8. García-León, D. et al. Current and projected regional economic impacts of heatwaves in Europe. *Nat. Commun.* **12**, 5807 (2021).
9. Ruffault, J. et al. Increased likelihood of heat-induced large wildfires in the Mediterranean Basin. *Sci. Rep.* **10**, 13790 (2020).
10. Brás, T. A., Seixas, J., Carvalhais, N. & Jägermeyr, J. Severity of drought and heatwave crop losses tripled over the last five decades in Europe. *Environ. Res. Lett.* **16**, 065012 (2021).
11. Sherwood, S. C. & Huber, M. An adaptability limit to climate change due to heat stress. *Proc. Natl. Acad. Sci.* **107**, 9552–9555 (2010).
12. Zscheischler, J. et al. A typology of compound weather and climate events. *Nat. Rev. Earth Environ.* **1**, 333–347 (2020).
13. Royé, D. et al. Effects of hot nights on Mortality in Southern Europe. *Epidemiology* **32**, 487–498 (2021).
14. Feller, U., Kingston-Smith, A. H. & Centritto, M. Editorial: abiotic stresses in agroecology: a challenge for whole plant physiology. *Front. Environ. Sci.* **5**, 13 (2017).
15. Wehner, M., Stone, D., Krishnan, H., AchutaRao, K. & Castillo, F. The deadly combination of heat and humidity in India and Pakistan in summer 2015. *Bull. Am. Meteorol. Soc.* **97**, S81–S86 (2016).
16. Robine, J. M. et al. Death toll exceeded 70,000 in Europe during the summer of 2003. *CR Biol.* **331**, 171–178 (2008).
17. Schuldt, B. et al. A first assessment of the impact of the extreme 2018 summer drought on central European forests. *Basic Appl. Ecol.* **45**, 86–103 (2020).
18. Toreti, A. et al. The exceptional 2018 European water seesaw calls for action on adaptation. *Earth's Future* **7**, 652–663 (2019).
19. AghaKouchak, A. et al. Climate extremes and compound hazards in a warming world. *Annu. Rev. Earth Planet. Sci.* **48**, 519–548 (2020).
20. de Ruiter, M. C. et al. Why we can no longer ignore consecutive disasters. *Earth's Future* **8**, e2019EF001425 (2020).
21. Bastos, A. et al. Vulnerability of European ecosystems to two compound dry and hot summers in 2018 and 2019. *Earth Syst. Dynam.* **12**, 1015–1035 (2021).
22. Callahan, C. W. & Mankin, J. S. Globally unequal effect of extreme heat on economic growth. *Sci. Adv.* **8**, 43 (2022).
23. Sutton, R. T. & Hodson, D. L. Ocean science: Atlantic ocean forcing of North American and European summer climate. *Science* **309**, 115–118 (2005).
24. Sutton, R. & Dong, B. Atlantic ocean influence on a shift in European climate in the 1990s. *Nat. Geosci.* **5**, 788–792 (2012).
25. Ghosh, R., Müller, W. A., Baehr, J. & Bader, J. Impact of observed North Atlantic multi-decadal variations to European summer climate: a linear baroclinic response to surface heat-ing. *Clim. Dyn.* **48**, 3547 (2017).
26. Lesk, C. & Anderson, W. Decadal variability modulates trends in concurrent heat and drought over global croplands. *Environ. Res. Lett.* **16**, 055024 (2021).
27. Qasmi, S., Sanchez-Gomez, E., Ruprich-Robert, Y., Boé, J. & Cassou, C. Modulation of the occurrence of heatwaves over the Euro-Mediterranean region by the intensity of the Atlantic multidecadal variability. *J. Clim.* **34**, 1099–1114 (2021).
28. Hodson, D. L. R. et al. Coupled climate response to Atlantic multidecadal variability in a multi-model multi-resolution ensemble. *Clim. Dyn.* **59**, 805–836 (2022).
29. Hellmich, L., Suarez-Gutierrez, L., Matei, D., and Müller, W. A.: Extremely Warm European Summers driven by Sub-Decadal North Atlantic Heat Inertia, EGU sphere [preprint], <https://doi.org/10.5194/egusphere-2023-653> (2023).
30. Samaniego, L. et al. Anthropogenic warming exacerbates European soil moisture droughts. *Nat. Clim. Change* **8**, 421–426 (2018).
31. Suarez-Gutierrez, L., Li, C., Müller, W. A. & Marotzke, J. Dynamical and thermodynamical drivers of variability in European summer heat extremes. *Clim. Dyn.* **54**, 4351–4366 (2020).
32. Raymond, C. et al. Increasing spatiotemporal proximity of heat and precipitation extremes in a warming world quantified by a large model ensemble. *Environ. Res. Lett.* **17**, 035005 (2022).
33. Bevacqua, E., Zappa, F., Lehner, F., Zscheischler, J. Precipitation trends determine future occurrences of compound hot–dry events. *Nat. Clim. Chang.* <https://doi.org/10.1038/s41558-022-01309-5> (2022).
34. van der Wiel, K., Batelaan, T. J. & Wanders, N. (2022) Large increases of multi-year droughts in north-western Europe in a warmer climate. *Clim. Dyn.* <https://doi.org/10.1007/s00382-022-06373-3> (2022).
35. Gao, M. et al. Footprints of Atlantic multidecadal oscillation in the low-frequency variation of extreme high temperature in the northern hemisphere. *J. Clim.* **32**, 791–802 (2019).
36. Borchert, L. et al. Decadal predictions of the probability of occurrence for warm summer temperature extremes. *Geophys. Res. Lett.* **16**, 14042–14051 (2019).
37. Müller, W. A., Borchert, L. & Ghosh, R. Observed subdecadal variations of European summer temperatures. *Geophys. Res. Lett.* **47**, e2019GL086043 (2020).
38. Ghosh, R., Müller, W. A., Eichhorn, A., Baher, J. & Bader, J. Atmospheric pathway between Atlantic multidecadal variability and European summer temperature in the atmospheric general circulation model ECHAM6. *Clim. Dyn.* **53**, 209–224 (2019).
39. Yeager, S. G. & Robson, J. I. Recent progress in understanding and predicting atlantic decadal climate variability. *Curr. Clim. Change Rep.* **3**, 112–127 (2017).
40. Perkins-Kirkpatrick, S. E. & Lewis, S. C. Increasing trends in regional heatwaves. *Nat. Commun.* **11**, 3357 (2020).
41. Maher, N. et al. The Max Planck Institute Grand Ensemble: enabling the exploration of climate system variability. *JAMES* **11**, 2050–2069 (2019).
42. Bevacqua, E. et al. Advancing research on compound weather and climate events via large ensemble model simulations. *Nat. Commun.* **14**, 2145 (2023).
43. Suarez-Gutierrez, L., Milinski, S. & Maher, N. Exploiting large ensembles for a better yet simpler climate model evaluation. *Clim. Dyn.* **57**, 2557–2580 (2021).
44. Wood, R. R., Lehner, F., Pendergrass, A. G. & Schlunegger, S. Changes in precipitation variability across time scales in multiple global climate model large ensembles. *Environ. Res. Lett.* **16**, 084022 (2021).
45. Mauritsen, T. et al. Developments in the MPI-M Earth System Model version 1.2 (MPI-ESM1.2) and its response to increasing CO₂. *J. Adv. Model. Earth Sys.* **11**, 998–1038 (2019).
46. Di Luca, A., Pitman, A. J. & de Elía, R. Decomposing temperature extremes errors in CMIP5 and CMIP6 models. *Geophys. Res. Lett.* **47**, e2020GL088031 (2020).
47. Schoetter, R., Cattiaux, J. & Douville, H. Changes of western European heat wave characteristics projected by the CMIP5 ensemble. *Clim. Dyn.* **45**, 1601–1616 (2015).
48. Russo, S. et al. Magnitude of extreme heat waves in present climate and their projection in a warming world. *J. Geophys. Res. Atmos.* **119**, 12,500–12,512 (2014).
49. Russo, S., Sillmann, J. & Fischer, E. M. Top ten European heatwaves since 1950 and their occurrence in the coming decades. *Environ. Res. Lett.* **10**, 124003 (2015).
50. Cornes, R. C., van der Schrier, G., van den Besselaar, E. J. M. & Jones, P. D. An ensemble version of the E-OBS temperature and precipitation data sets. *J. Geophys. Res. Atmos.* **123**, 9391–9409 (2018).
51. Bachmair, S., Tanguy, M., Hannaford, J. & Stahl, K. How well do meteorological indicators represent agricultural and forest drought across Europe? *Environ. Res. Lett.* **13**, 034042 (2018).
52. Hanel, M. et al. Revisiting the recent European droughts from a long-term perspective. *Sci. Rep.* **8**, 9499 (2018).
53. Stull, R. Wet-bulb temperature from relative humidity and air temperature. *J. Appl. Meteorol. Climatol.* **50**, 2267–2269 (2011).
54. Buzan, J. R., Oleson, K. & Huber, M. Implementation and comparison of a suite of heat stress metrics within the Community Land Model version 4.5. *Geosci. Model Dev.* **8**, 151–170 (2015).
55. Russo, E. & Domeisen, D. I. V. Increasing intensity of extreme heatwaves: the crucial role of metrics. *Geophys. Res. Lett.* **50**, e2023GL103540 (2023).
56. Deser, C. & Phillips, A. S. Defining the internal component of Atlantic Multidecadal Variability in a changing climate. *Geophys. Res. Lett.* **48**, e2021GL095023 (2021).
57. Schulzweida, Uwe. CDO User Guide (2.1.0). Zenodo. <https://doi.org/10.5281/zenodo.7112925> (2022).

Acknowledgements

This project was supported by the Max Planck Society for the Advancement of Science and by the German Ministry of Education and Research (BMBF) under the ClimXtreme project, subproject DecHeat (Grant number 01LP1901F). L.S.G. has also received funding from the European Union's Horizon Europe Framework Programme under the Marie Skłodowska-Curie grant agreement No 101064940. We thank Leonard Borchert and three anonymous reviewers for providing insightful comments and suggestions to improve this work. We acknowledge Sebastian Brune and Johanna Baehr for producing and processing the historical and RCP4.5 MPI-GE simulations used in this study, and the Swiss National Computing Centre (CSCS) and the German Climate Computing Center (DKRZ) for providing the necessary computational resources. This work used resources of the Deutsches Klimarechenzentrum (DKRZ) granted by its Scientific Steering Committee (WLA) under project ID bb1152.

Author contributions

L.S.G. designed and performed the analysis and drafted the manuscript, W.A.M. and J.M. contributed to shaping the research and to the interpretation of the results, and provided feedback on the manuscript.

Funding

Open Access funding enabled and organized by Projekt DEAL.

Competing interests

The authors declare no competing interests.

Additional information

Supplementary information The online version contains supplementary material available at <https://doi.org/10.1038/s43247-023-01075-y>.

Correspondence and requests for materials should be addressed to Laura Suarez-Gutierrez.

Peer review information *Communications Earth & Environment* thanks Luke Harrington, Ana Oliveira and the other, anonymous, reviewer(s) for their contribution to the peer review of this work. Primary Handling Editor: Aliénor Lavergne. A peer review file is available

Reprints and permission information is available at <http://www.nature.com/reprints>

Publisher's note Springer Nature remains neutral with regard to jurisdictional claims in published maps and institutional affiliations.



Open Access This article is licensed under a Creative Commons Attribution 4.0 International License, which permits use, sharing, adaptation, distribution and reproduction in any medium or format, as long as you give appropriate credit to the original author(s) and the source, provide a link to the Creative Commons license, and indicate if changes were made. The images or other third party material in this article are included in the article's Creative Commons license, unless indicated otherwise in a credit line to the material. If material is not included in the article's Creative Commons license and your intended use is not permitted by statutory regulation or exceeds the permitted use, you will need to obtain permission directly from the copyright holder. To view a copy of this license, visit <http://creativecommons.org/licenses/by/4.0/>.

© The Author(s) 2023